Published OnlineFirst February 7, 2012; DOI: 10.1158/1535-7163.MCT-11-0891

Preclinical Development

Molecular Cancer Therapeutics

Nanobodies Targeting the Hepatocyte Growth Factor: Potential New Drugs for Molecular Cancer Therapy

Maria J.W.D. Vosjan[1], Jo Vercammen[3], Joost A. Kolkman[3], Marijke Stigter-van Walsum[1], Hilde Revets[3], and Guus A.M.S. van Dongen[1,2]

Abstract

Hepatocyte growth factor (HGF) and its receptor c-Met are associated with increased aggressiveness of tumors and poor prognostic outcome of patients with cancer. Here, we report the development and characterization of therapeutic anti-HGF (αHGF)-Nanobodies and their potential for positron emission tomographic (PET) imaging to assess HGF expression *in vivo*. Two αHGF-Nanobodies designated 1E2 and 6E10 were identified, characterized, and molecularly fused to an albumin-binding Nanobody unit (Alb8) to obtain serum half-life extension. The resulting Nanobody formats were radiolabeled with the positron emitter zirconium-89 (^{89}Zr, $t_1/_2 = 78$ hours), administered to nude mice bearing U87 MG glioblastoma xenografts, and their biodistribution was assessed. In addition, their therapeutic effect was evaluated in the same animal model at doses of 10, 30, or 100 μg per mouse. The ^{89}Zr-Nanobodies showed similar biodistribution with selective tumor targeting. For example, 1E2-Alb8 showed decreased blood levels of 12.6%ID/g ± 0.6%ID/g, 7.2%ID/g ± 1.0%ID/g, 3.4%ID/g ± 0.3%ID/g, and 0.3%ID/g ± 0.1%ID/g at 1, 2, 3, and 7 days after injection, whereas tumor uptake levels remained relatively stable at these time points: 7.8%ID/g ± 1.1%ID/g, 8.9%ID/g ± 1.0%ID/g, 8.7%ID/g ± 1.5%ID/g, and 7.2%ID/g ±1.6%ID/g. Uptake in normal tissues was lower than in tumor, except for kidneys. In a therapy study, all Nanobody-treated mice showed tumor growth delay compared with the control saline group. In the 100-μg group, four of six mice were cured after treatment with 1E2-Alb8 and 73 days follow-up, and three of six mice when treated with 6E10-Alb8. These results provide evidence that Nanobodies 1E2-Alb8 and 6E10-Alb8 have potential for therapy and PET imaging of HGF-expressing tumors. *Mol Cancer Ther; 11(4); 1017–25. ©2012 AACR.*

Introduction

Hepatocyte growth factor (HGF), also known as scatter factor, is secreted as a single-chain, inactive polypeptide by mesenchymal cells, and is cleaved by serine proteases into a 69-kDa α-chain and 34-kDa β-chain (1–3). HGF is the only known ligand for the c-Met receptor. The c-Met receptor is expressed during embryogenesis and adulthood in the epithelial cells of many organs like liver, prostate, pancreas, muscle, kidney, and bone marrow. In tumor cells, c-Met activation triggers diverse series of signaling cascades resulting in cell growth, proliferation, invasion, metastasis formation, and escape from apoptosis (3). Overexpression of HGF and c-Met is associated with increased aggressiveness of tumors and poor prognostic outcome of patients with cancer (www.vai.org/vari/metandcancer; ref. 4). HGF and c-Met expression have been observed in most solid tumors. Blocking the soluble factor might be a beneficial strategy over blocking the c-Met receptor, as HGF is expected to be highly expressed in the tumor only, is easily accessible for Nanobodies, and is the only know ligand for the c-Met receptor. The possibility for success with targeting soluble factors has been illustrated with the anti-VEGF antibody bevacizumab (5).

The last decades several pharmaceutical companies have been actively involved in the development of therapeutic tyrosine kinase inhibitors and monoclonal antibodies (mAb) that antagonize c-Met activation. At least 16 agents have been or are being evaluated in the clinic at the moment, as reviewed by Liu and colleagues (6). To their and our knowledge, 3 anti-HGF (αHGF) mAbs are under clinical development at the moment, including AMG102 (rilotumumab), a humanized antihuman HGF IgG2 from Amgen, AV-299 from Schering/Aveo, and TAK-701 from Millennium.

In the present study, we introduce αHGF-Nanobodies. Nanobodies are derived from a unique antibody format

Authors' Affiliations: Departments of [1]Otolaryngology/Head and Neck Surgery and [2]Nuclear Medicine & PET Research, VU University Medical Center, Amsterdam, The Netherlands; and [3]Ablynx NV, Ghent, Belgium

Note: Supplementary material for this article is available at Molecular Cancer Therapeutics Online (http://mct.aacrjournals.org/).

Corresponding Author: Guus A.M.S. van Dongen, Department of Otolaryngology/Head and Neck Surgery, VU University Medical Center, De Boelelaan 1117, PO Box 7057, Amsterdam 1007 MB, The Netherlands. Phone: 31-20-4440953; Fax: 31-20-4443688; E-mail: gams.vandongen@vumc.nl

doi: 10.1158/1535-7163.MCT-11-0891

Published OnlineFirst February 7, 2012; DOI: 10.1158/1535-7163.MCT-11-0891

that is present in species from the family of *Camelidae*, including llama, camel, and dromedary. These animals contain, besides their conventional antibody repertoire, an antibody class consisting of heavy chain–only antibodies (7–9). The variable region of the heavy chain–only antibodies (VHH) represents the complete binding unit of the antibody and is also termed Nanobody (Nanobody is a registered trademark of Ablynx NV). Unique features of the Nanobody technology platform in comparison to conventional mAb technology are rapid drug development, biophysical, and chemical robustness and the potential to target intractable targets for antibodies including G-protein–coupled receptors (GPCR) and ion channels (9). Particularly attractive is the ability to design modular drugs based on 15-kDa Nanobody building blocks combined with each other, with other protein domains or with other molecules or drugs. Nanobodies have been combined in a wide range of formats, including multivalent (multiple Nanobodies with identical-binding sites for the same antigen; refs. 10, 11), biparatopic (2 Nanobodies binding to 2 different epitopes on the same antigen; refs. 12, 13), and bispecific (Nanobodies binding to 2 different antigens; refs. 13, 14) molecules. These formats are easy to construct and the modular proteins can often be expressed at high levels in bacteria or yeast. As a result of this formatting flexibility, the range of therapeutic applications for Nanobodies seems to be beyond that possible for conventional antibodies and antibody fragments. Nanobodies can also be tailored for a half-life varying from less than 2 hours up to a few weeks, by choosing from a wide range of half-life extension technologies. This versatility increases the number of therapeutic options available to Nanobodies ranging from acute to chronic indications where a monthly or bimonthly dosing regimen may be desirable.

Initial biodistribution studies with monospecific anti-EGFR (αEGFR)-Nanobodies in tumor-bearing mice showed, as expected, rapid blood clearance with a serum half-life time of less than an hour and low tumor uptake (15–17). Therefore, monospecific Nanobodies do not seem to be qualified for long-term blockage of growth factors and their receptors. Improvement of the pharmacokinetic and dynamic properties of otherwise short-live molecules can be achieved by fusing an anti-albumin unit (αAlb) to the Nanobody, as described by Tijink and colleagues (18). They compared the biodistribution of a bivalent αEGFR-Nanobody (αEGFR-αEGFR) with a trivalent Nanobody construct containing the αAlb-unit (αEGFR-αEGFR-αAlb) in nude mice bearing A431 tumors. Tumor uptake of αEGFR-αEGFR-αAlb was significantly higher than of αEGFR-αEGFR: 35.2%ID/g ± 7.5%ID/g vs. 5.0%ID/g ± 1.4%ID/g. What is more, biodistribution of αEGFR-αEGFR-αAlb (50 kDa) was comparable with cetuximab (150 kDa), while it showed faster and deeper tumor penetration. The therapeutic potential of αEGFR-Nanobodies in comparison with conventional αEGFR mAbs was shown by Roovers and colleagues (13).

In the present study, we developed and characterized 2 αHGF-Nanobodies 1E2-Alb8 and 6E10-Alb8 for their capacity to inhibit binding of HGF to the c-Met receptor and for their potential in diagnosis and therapy of cancer. After labeling with the positron emitter zirconium-89 the Nanobodies were evaluated in biodistribution studies in nude mice bearing U87 MG glioblastoma xenografts. Besides that, αHGF-Nanobodies were tested as therapeutic agents in the same animal model.

Materials and Methods

Details of production and selection of αHGF-Nanobodies are presented in the Supplementary Materials.

Selective binding of Nanobodies to human HGF in ELISA

Nanobody-containing periplasmic extracts were analyzed for their ability to bind HGF. HGF (294-HG/CF, R&D systems) was coated on ELISA plates at 2 μg/mL. Plates were washed and subsequently blocked using PBS with 1% casein. Periplasmic extracts of individual clones, prediluted 1:10 in PBS/1% casein/0.05% Tween, were added and plates were incubated at room temperature for 2 hours. Binding to immobilized HGF was detected using mouse anti-c-Myc mAb, followed by a horseradish peroxidase–conjugated rabbit-antimouse (human and bovine serum protein preabsorbed) mAb for detection. Individual clones were scored as putative HGF binders if the clones showed high-optical densities in the assay. Overall, more than 90% of the clones were able to bind HGF.

Kinetic measurement Nanobody-antigen K_d values

Kinetic (k_a and k_d) and affinity constants (K_d) of individual purified Nanobodies were determined by surface plasmon resonance on a Biacore T100 instrument. Human HGF (R&D systems) was amine coupled to a CM5 sensor chip at a density of 2,500 relative units. Remaining reactive groups were inactivated with ethanolamine. Nanobody binding was assessed at varying concentrations ranging from 500 to 15 nmol/L. Each sample was injected for 2 minutes at a flow rate of 45 μL/min to allow binding to chip-bound antigen. Next, binding buffer without Nanobody was sent over the chip at the same flow rate to allow dissociation of bound Nanobody. After 10 minutes, remaining bound analyte was removed by injecting regeneration solution (1 mol/L NaCl, 50 mmol/L NaOH). Binding–dissociation curves were used to calculate K_{off} values.

Receptor–ligand-binding assay

Serial dilutions of purified Nanobodies were analyzed for their ability to block the interaction of human HGF with c-Met-Fc by the AlphaScreen assay (PerkinElmer). In brief, 5 μL of prediluted individual Nanobody clones were incubated with 3 nmol/L biotinylated HGF, 2 nmol/L c-Met-Fc, streptavidin-coated donor beads, and antihuman IgG1 Fc Nanobody covalently coupled

Published OnlineFirst February 7, 2012; DOI: 10.1158/1535-7163.MCT-11-0891

Alphascreen acceptor beads. mAb clone 24612 (R&D systems) known to inhibit the HGF/c-Met-Fc interaction was used as a positive control. Assays were read in an Envision AlphaScreen option fitted multimode reader (PerkinElmer).

Cells and culture

U-87 MG (human glioblastoma), Bx-PC3 (human prostate carcinoma), and A549 (human alveolar basal epithelial cell carcinoma) cells were all obtained from the American Type Culture Collection (www.ATCC.com) and cultured according to their recommendations. Cell lines were not authenticated by the authors.

Functional cell assays: c-Met phosphorylation assay

A549 cells were plated in growth medium, and after 24 hours the cells were starved for 18 to 20 hours. c-Met phosphorylation was stimulated with 5 nmol/L human HGF for 15 minutes. Each of the half-life extended Nanobodies 1E2-Alb8 and 6E10-Alb8 was prepared as a 3-point serial dilution series in the stimulation medium before adding to the cells. Following the 15-minute incubation, cells were immediately placed on ice and lysed in RIPA buffer (Cell Signaling Technology). Quantification of phosphorylated (Tyr1349) and total c-Met was conducted by the MSD 96-Well MULTI-SPOT Phospho (Tyr1349)/Total c-Met Assay according to the manufacturer's instructions. IC_{50} values were calculated with the 4-Parameter Logistic equation (GraphPad Prism)

Functional cell assays: proliferation assay

BxPc3 cells were seeded in cell culture E-plates at a cell density of 10,000 cells per well and incubated overnight in culture medium at 37°C and 5% CO_2. Cells were then starved with medium containing 1% ITS (insulin, transferrin, and selenium) for 4 hours after which 0.6 nmol/L HGF was added together with serial dilutions of Nanobodies 1E2-Alb8 and 6E10-Alb8. The cell growth curves were automatically recorded on the xCELLigence System (Roche Applied Sciences) in real-time. The cell index was followed for 3 days.

Preparation of ^{89}Zr-1E2-Alb8 and ^{89}Zr-6E10-Alb8

For preparation of the ^{89}Zr conjugates, the ^{89}Zr was coupled to the Nanobody by use of the bifunctional chelate *p*-isothiocyanatobenzyl desferrioxamine (Df-Bz-NCS, catalog no. # B705; Macrocyclics), essentially as described by Vosjan and colleagues (19).

Quality control of ^{89}Zr-1E2-Alb8 and ^{89}Zr-6E10-Alb8

All radioactive conjugates were analyzed by instant thin-layer chromatography to determine the labeling efficiency and radiochemical purity. The integrity of the Nanobody was analyzed via size exclusion chromatography by high-performance liquid chromatography (HPLC) and SDS-PAGE followed by phosphor imager analysis (Storm820; GE Healthcare). Immunoreactivity was determined by a HGF-coated ELISA essentially as described by Collingridge and colleagues (20).

Biodistribution study

The distribution of ^{89}Zr-labeled αHGF-Nanobodies was examined in nude mice (HSD: Athymic Nude-Foxn1^{nu}, 20–30 g; Harlan Laboratories) inoculated subcutaneously with 2×10^6 U87 MG cells at 2 lateral sides. These animal experiments were done according to NIH Principles of Laboratory Animal Care and Dutch national law (Wet op de dierproeven, Stb 1985, 336).

Mice bearing U87 MG xenografts (size, ~100 mm^3) were injected with 0.37 MBq ^{89}Zr-Df-Bz-NCS-1E2-Alb8 or 0.37 MBq ^{89}Zr-Df-Bz-NCS-6E10-Alb8 via the retro-orbital plexus. Unlabeled Nanobody was added to the injection mixture to obtain a final dose of 30 μg per mouse. At 1, 2, 3, or 7 days after injection, 5 mice per group were anesthetized, bled, killed, and dissected. Blood, tumor, and normal tissues were weighed and radioactivity was measured in a gamma counter (Wallac). Radioactivity uptake for each sample was calculated as the percentage of the injected dose per gram of tissue (%ID/g).

In addition, a Nanobody dose-diminishing study was conducted. To this end, 5, 10, 20, and 30 μg of ^{89}Zr-labeled 1E2-Alb8 (0.23–0.83 MBq) was injected in mice bearing U87 MG xenografts, and at 3 days after injection 5 mice per group were examined as described earlier.

Blood kinetics

Blood concentrations of αHGF-Nanobodies were examined in 2 groups of 2 mice. One group of tumor-bearing mice received 0.37 MBq ^{89}Zr-1E2-Alb8 (30 μg) whereas the other group received 0.37 MBq ^{89}Zr-6E10-Alb8 (30 μg). Blood was collected at 1 and 3 hours and at 1, 2, 3, and 7 days after injection by tail laceration, and radioactivity was measured in a gamma counter. Radioactivity for each sample was calculated as %ID/g.

Therapy study

The therapeutic effectiveness of the αHGF-Nanobodies was studied in the same nude mice model as described for the biodistribution study. For this purpose, 7 groups of 6 mice with established U87 MG xenografts were used. The mean tumor size at the start of the study was approximately 100 mm^3 and was similar for the different treatment groups. All mice received i.p. treatment 3 times a week for 5 weeks. Group 1 was the control group and received 200 μL of saline solution per treatment. Group 2, 3, and 4 received 10, 30, and 100 μg of Nanobody 1E2-Alb8, respectively. Group 5, 6, and 7 received 10, 30, and 100 μg of Nanobody 6E10-Alb8, respectively. Body weight and tumor volume were measured 3 times a week up to 73 days after end of treatment.

Statistical analysis

Biodistribution and therapy experiments were statistically analyzed with SPSS 15.0 software using Student *t* test for unpaired data. Two-sided significance levels were

Published OnlineFirst February 7, 2012; DOI: 10.1158/1535-7163.MCT-11-0891

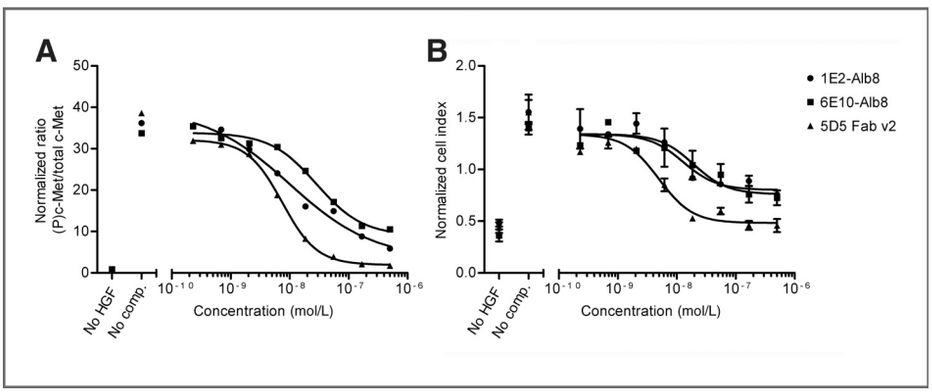

Figure 1. αHGF-Nanobodies neutralize HGF-mediated cellular functions. A, αHGF-Nanobodies neutralize HGF-mediated c-Met phosphorylation. The percentage inhibition of c-Met phosphorylation was measured over an 8-point dose–response of each Nanobody by an enhanced chemiluminescence assay. B, αHGF-Nanobodies inhibit HGF-dependent growth of PC3 cells. The viability of PC3 cells cultured more than 3 days in the presence of 0.6 nmol/L HGF was measured over an 8-point dose–response of each Nanobody via impedance measurement. Anti-c-Met 5D5 Fab was used as a positive control.

calculated, and $P < 0.01$ was considered statistically significant. Survival was calculated using Kaplan–Meier curves.

Results

Generation and characterization of αHGF-Nanobodies 1E2 and 6E10

To obtain antagonistic Nanobodies specific for HGF, phage Nanobody repertoires were synthesized from peripheral blood lymphocytes from llamas immunized with HGF. After panning to immobilized HGF, single clones were screened as periplasmic extracts for HGF reactivity by ELISA. Approximately 90% of the clones tested were found to bind HGF. In a next step, their potential to inhibit HGF/c-Met interaction was assessed in an AlphaScreen and resulted in a final panel of 12 clones, which showed good inhibition of the HGF/c-Met interaction. Using a Biacore T100, we analyzed the affinity of the Nanobodies to HGF. On the basis of these analyses, Nanobodies 1E2 and 6E10 were selected from this panel for further characterization. These selected Nanobodies inhibited binding of HGF to c-Met with IC_{50} values in the low nanomolar range (1.8 nmol/L for 1E2 and 3 nmol/L for 6E10 Nanobody) though 100% inhibition was not achieved. The kinetic parameters of Nanobody-antigen showed that both Nanobodies displayed low nmol/L affinity constants (1.36 nmol/L for 1E2 and 1.14 nmol/L for 6E10 Nanobody).

Reformatting of Nanobodies for *in vivo* use and *in vitro* characterization of these formats

To increase the *in vivo* half-life of the αHGF-Nanobodies, bispecific formats were generated whereby the αHGF-Nanobodies were genetically linked to a Nanobody with specificity to serum albumin (Alb8). These bispecific Nanobodies were produced as Myc-His6 tagged proteins in *Escherichia coli* and analyzed for their potential to neutralize HGF-mediated c-Met phosphorylation. A549 cells do not express HGF; thus, this assay mimicked a paracrine model of ligand-mediated receptor activation. When Nanobody 1E2-Alb8 or 6E10-Alb8 was introduced into HGF-containing medium before addition to the cells, c-Met phosphorylation was inhibited in a dose-dependent manner though less efficient than control anti-c-Met 5D5 Fab (Fig. 1A).

We next measured inhibition of HGF-induced proliferation of Bx-PC3 cells. Also here, a dose-dependent inhibition was observed when the Nanobodies were added to the Bx-PC3 cells in culture, but also here inhibition was less efficient than with the anti-c-Met 5D5 Fab control (Fig. 1B).

Radiolabeling and quality control of ^{89}Zr-1E2-Alb8 and ^{89}Zr-6E10-Alb8

Labeling of both Nanobodies with ^{89}Zr resulted in overall labeling yields of 75% to 90%, after PD-10 column purification. Radiochemical purity was always more than 97%. Integrity of the Nanobodies was optimal as determined by HPLC and SDS-PAGE. Immunoreactivity of ^{89}Zr-1E2-Alb8 and ^{89}Zr-6E10-Alb8 was similar to that of the reference ^{131}I-labeled αHGF-Nanobodies (∼50%).

Biodistribution study

For biodistribution studies, nude mice bearing U87 MG xenografts were injected with either ^{89}Zr-1E2-Alb8 or ^{89}Zr-6E10-Alb8. Biodistributions at 1, 2, 3, or 7 days after injection are shown in Fig. 2. Both αHGF-Nanobodies showed similar biodistributions with selective tumor uptake, no significant differences were observed ($P > 0.01$). Whereas blood levels gradually decreased over time, tumor uptake remained relatively stable. Blood levels were 12.6%ID/g ± 0.7%ID/g, 7.2%ID/g ± 1.0%ID/g, 3.4%ID/g ± 0.3%ID/g, and 0.3%ID/g ± 0.1%ID/g for ^{89}Zr-1E2-Alb8 and 13.1%ID/g ± 0.6%ID/g, 7.4%ID/g ± 0.6%ID/g, 3.5%ID/g ± 0.5%ID/g, and 0.5%ID/g ± 0.1%ID/g for ^{89}Zr-6E10-Alb8 at 1, 2, 3, and 7 days after injection, respectively. Tumor uptake at these time points was 7.8%ID/g ± 1.1%ID/g, 8.9%ID/g ± 1.0%ID/g,

Published OnlineFirst February 7, 2012; DOI: 10.1158/1535-7163.MCT-11-0891

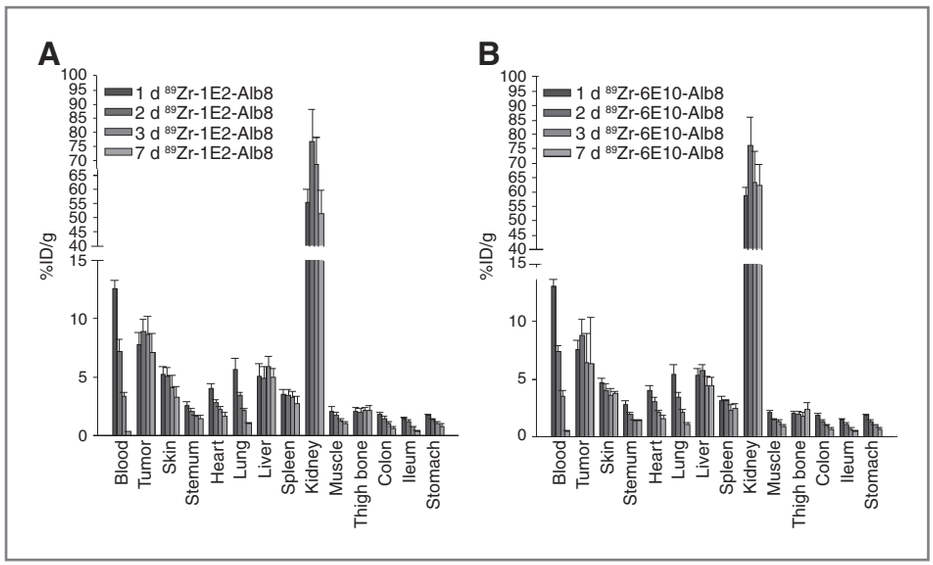

Figure 2. Biodistribution of αHGF-Nanobodies ^{89}Zr-1E2-Alb8 (A) and ^{89}Zr-6E10-Alb8 (B) in nude mice bearing U87 MG xenografts at 1, 2, 3, and 7 days after injection Data are presented as average of 5 animals and SDs. No significant differences in uptake between both Nanobodies were observed ($P < 0.01$).

8.7%ID/g ± 1.5%ID/g, and 7.2%ID/g ± 1.6%ID/g for ^{89}Zr-1E2-Alb8 and 7.5%ID/g ± 0.8%ID/g, 8.8%ID/g ± 1.3%ID/g, 6.5%ID/g ± 2.5%ID/g, and 6.3%ID/g ± 4.0%ID/g at 1, 2, 3, and 7 days after injection, respectively, for ^{89}Zr-6E10-Alb8. Tumor uptake was higher than in normal organs, except for kidneys. The latter is typical for small proteins, which are rapidly cleared via the kidneys.

Dose-diminishing study

A dose-diminishing study was conducted with ^{89}Zr-1E2-Alb8 to determine the optimal Nanobody dose for *in vivo* imaging. Nude mice bearing U87 MG xenografts were injected with 0.32 ± 0.01, 0.47 ± 0.01, 0.47 ± 0.01, or 0.83 ± 0.01 MBq ^{89}Zr-1E2-Alb8, containing 5, 10, 20, or 30 μg 1E2-Alb8, respectively. Three days after injection, similar biodistribution was seen for all dose groups (Fig. 3). No significant differences were observed in tumor uptake, being 8.2%ID/g ± 1.2%ID/g, 8.1%ID/g ± 1.3%ID/g, 6.3%ID/g ± 1.7%ID/g, and 6.9%ID/g ± 1.1%ID/g for the 5, 10, 20, and 30 μg dose groups, respectively. High uptake in kidneys was observed for all dose groups. Also no significant differences were observed between the different dose groups ($P > 0.01$).

Blood kinetics in mice

Blood kinetics of ^{89}Zr-1E2-Alb8 (30 μg) and ^{89}Zr-6E10-Alb8 (30 μg) appeared to be similar (Fig. 4). Blood levels of Nanobody constructs were 41.7%ID/g ± 0.6%ID/g and 35.1%ID/g ± 1.48%ID/g 1 hour after injection for ^{89}Zr-1E2-Alb8 and ^{89}Zr-6E10-Alb8, respectively and slowly decreased from 4.3%ID/g ± 0.1%ID/g to 0.3%ID/g ± 0.1%ID/g between 72 and 168 hours after injection for ^{89}Zr-1E2-Alb8 and from 4.2%ID/g ± 0.1%ID/g to 0.5%ID/g ± 0.1%ID/g for ^{89}Zr-6E10-Alb8.

Therapy study

Mice receiving Nanobodies showed tumor growth delay in comparison to the control PBS group, whereas no toxicity was observed (Fig. 5A). Within the treatment period of 35 days all control mice were sacrificed because of the large volumes of the tumors. Mice receiving the lowest dose (10 μg) had minimal benefit whereas the

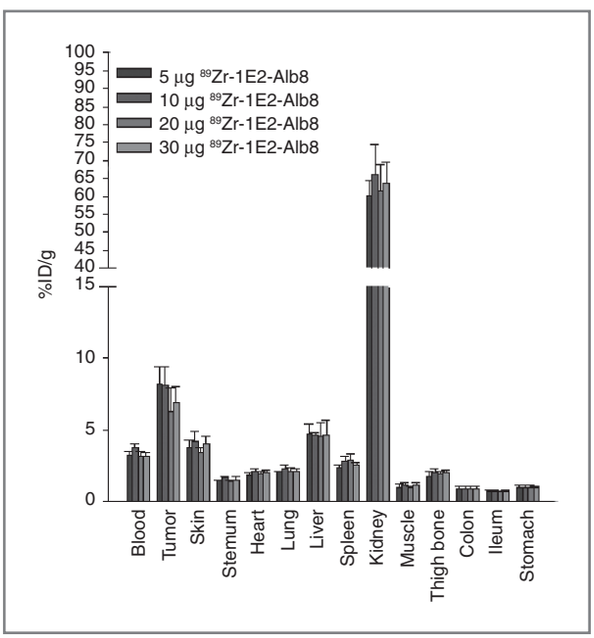

Figure 3. Biodistribution of αHGF-Nanobody ^{89}Zr-1E2-Alb8 in nude mice bearing U87 MG xenografts at 3 days after injection with different amounts of Nanobody. Data are presented as average of 5 animals and SD. No significant differences were observed between the dose groups ($P < 0.01$).

Published OnlineFirst February 7, 2012; DOI: 10.1158/1535-7163.MCT-11-0891

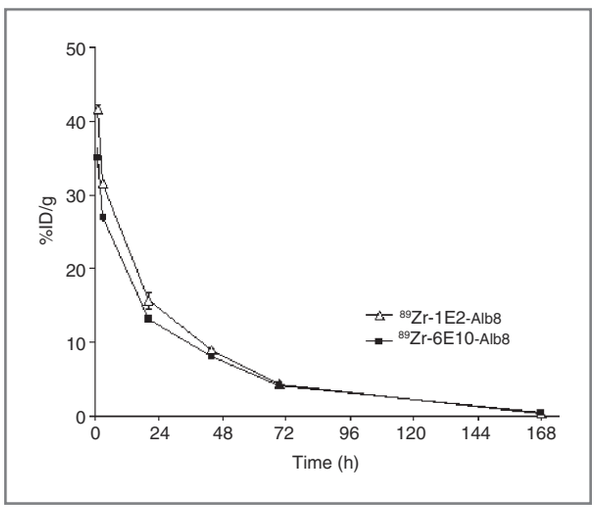

Figure 4. Blood kinetics of ^{89}Zr-labeled 1E2-Alb8 and 6E10-Alb8 in nude mice bearing U87 MG xenografts ($n = 2$ per group) up to 7 days after injection. Total administered dose, 30 μg.

intermediate and highest dose groups (30 and 100 μg) showed extensive tumor growth delay.

At the end of treatment (day 35) only mice in the intermediate and highest dose groups were alive, and followed till day 108 after start of treatment. At the end of the study 4 of 6 mice (7 of 11 tumors) were cured in the group receiving 100 μg 1E2-Alb8, and 3 of 6 mice (6 of 11 tumors) in the group receiving 100 μg 6E10-Alb8, whereas 3 of 6 mice (5 of 11 tumors) were cured in the group receiving 30 μg 1E2-Alb8. In contrast, all mice in the group receiving 30 μg 6E10-Alb8 faced regrowth of tumors during follow-up (Fig. 5B and C).

Discussion

Targeting of the HGF/c-Met pathway is considered to be a promising approach for treatment of cancer. Activation of c-Met by its ligand HGF can lead to multiple cellular responses, including invasion, proliferation, and motility. In this study, we described the development of 2 Nanobodies designated 1E2 and 6E10, with low nanomolar affinity for HGF, that have the capacity to inhibit binding of HGF to the c-Met receptor. By genetically linking these αHGF-Nanobodies to a Nanobody unit with specificity for serum albumin (Alb8; refs. 13, 18, 21), 1E2-Alb8 and 6E10-Alb8 were obtained. Nanobodies were radiolabeled with ^{89}Zr to enable accurate assessment of *in vivo* biodistribution either by taking biopsies as carried out herein or alternatively by noninvasive positron emission tomographic (PET) imaging as is foreseen in future clinical trials. ^{89}Zr-1E2-Alb8 and ^{89}Zr-6E10-Alb8 showed a similar extended serum half-life as has been previously described for αEGFR-Nanobodies (18), with blood levels of 10%ID/g to 15%ID/g at 24 hours after injection. Biodistribution studies also showed selective accumulation

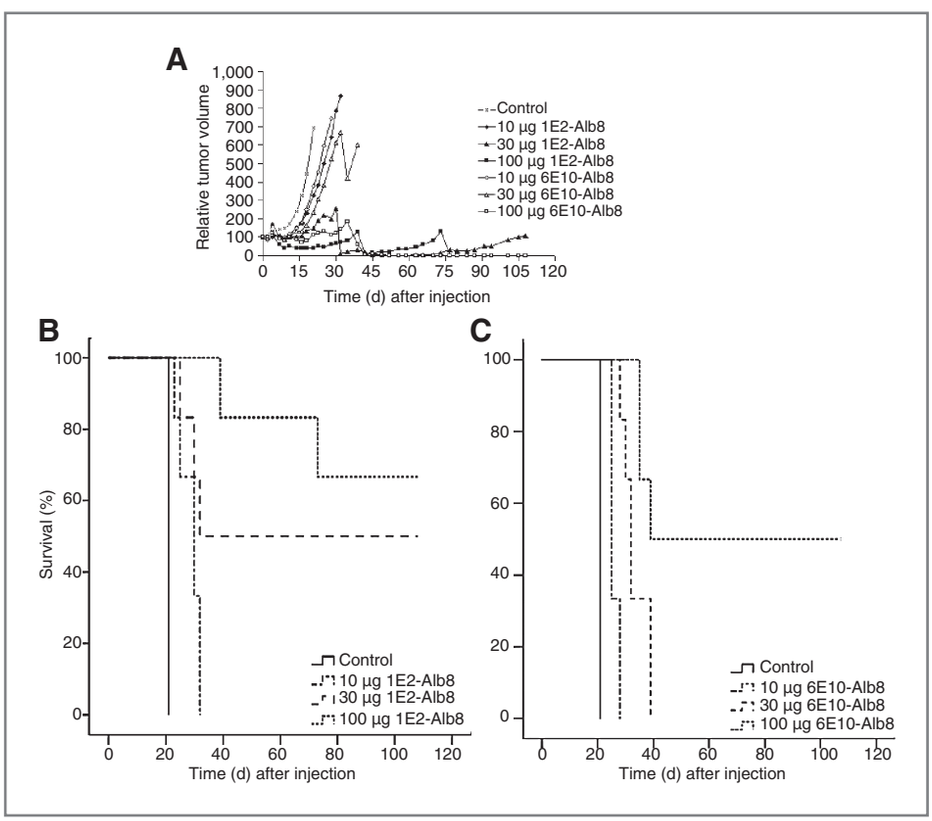

Figure 5. Therapy study with αHGF-Nanobodies 1E2-Alb8 and 6E10-Alb8 in nude mice bearing U87 MG glioblastoma xenografts (A). Treatment was 3 times a week for 5 weeks. Kaplan–Meier survival curves of nude mice treated with different amounts of 1E2-Alb8 (B) or 6E10-Alb8 (C). Treatment with all Nanobody concentrations caused significant tumor growth delay of the established tumors after day 6 ($P < 0.01$) and curative responses after treatment with 30 or 100 μg 1E2-Alb8, or 100 μg 6E10-Alb8.

Published OnlineFirst February 7, 2012; DOI: 10.1158/1535-7163.MCT-11-0891

of ^{89}Zr-1E2-Alb8 and ^{89}Zr-6E10-Alb8 in HGF-producing U87 MG xenografts. Besides this, both αHGF-Nanobodies were able to inhibit tumor growth in U87 MG tumor–bearing nude mice, and upon treatment by 100 μg i.p. injections, 3 times a week for 5 weeks, cures were observed in 4 of 6 mice with 1E2-Alb8 and in 3 of 6 mice with 6E10-Alb8.

Several therapy studies with αHGF mAbs have been conducted in U87 MG tumor–bearing mice in the past, and this allows ranking of the potency of the αHGF-Nanobodies described herein. In 2001, Cao and colleagues (22) reported for the first time on HGF-neutralizing mAbs capable for exerting antitumor activity. A mixture of 3 antibodies (200 μg per mouse every day until day 20; i.p. or intratumoral injection) was used for therapy in mice that had been injected one day earlier with C-127 or U118 cells. C-127 are mouse breast tumor cells transformed with human HGF and mouse Met, whereas U118 are human glioblastoma cells showing autocrine HGF production. Inhibition of tumor outgrowth was observed for both cell lines. The same mAb mixture (200 μg per mouse every 2 days until day 10; i.p. or intratumoral injection) also caused tumor growth inhibition in mice bearing established U118 xenografts (average size of 100 mm^3), however, no tumor regression or cures were observed. In these studies a mixture of 3 mAbs was used for therapy, because *in vitro* studies had shown that no single mAb appeared capable of neutralizing the activity of HGF. The authors, therefore, postulated that a minimum of 3 HGF epitopes have to be blocked to prevent c-Met tyrosine kinase activation and to exert antitumor activity.

In 2006, Burgess and colleagues (23) introduced fully human mAbs directed to an epitope in the β-chain of HGF, mAb AMG102 included, which showed inhibition of HGF-driven c-Met phopshorylation and of tumor growth as single agents. For their *in vivo* experiments they used established xenografts with an average size of 180 mm^3 derived from the glioblastoma cell lines U87 MG and U118, both expressing human HGF and c-Met. The most potent mAb showed significant growth inhibition and tumor regression when administered at a dose of 10 or 30 μg twice a week, and 7 of 10 animals in the 30-μg dose group had no measurable tumor mass at the end of the experiment. Because of the very short follow-up time of 17 days after start of therapy, and the lack of withdrawal from therapy, it did not become clear from these studies whether cures could be obtained like in our studies with the same Nanobody dose in the same xenograft model.

In later studies, the group of Burgess showed the potential of using αHGF therapy in combination approaches for treatment of glioblastoma (24). In the above described U87 MG xenograft model, low doses of AMG102 (3 μg twice a week) enhanced the efficacy of temozolomide or docetaxel. What is more, a first in human phase I trial in patients with advanced solid tumors showed that AMG102 is safe and well tolerated, with a linear pharmacokinetic profile within the investigated dose range (up to 20 mg/kg intravenous every 2 weeks; ref. 25). Despite the fact that the maximum-tolerated dose was not reached, 16 of 23 evaluable patients had a best response of stable disease with a progression-free survival ranging from 7.9 to 40 weeks. Above data indicate that αHGF-based therapy has clinical potential. Recently, indication was made that the HGF/c-Met pathway is also a therapeutic target in metastatic renal cell carcinoma. Nevertheless, Schöffski and colleagues showed that no significant growth inhibition occurred with AMG102 (26). Similarly, HGF and its receptor c-Met have been implicated in the pathogenesis of glioblastoma, but Wen (27) and colleagues showed in a phase II study that AMG102 monotherapy treatment at doses up to 20 mg/kg was not associated with significant antitumor activity in the selected patient groups.

Besides these mAbs, studies were conducted with the murine mAb L2G7 in 3 different established tumor models including U87 MG (28, 29). Treatment with 50 or 100 μg L2G7, i.p. twice weekly, was started when tumor volume reached approximately 50 mm^3 and resulted in inhibited tumor growth and regressions. Because of the short follow-up period (till day 40 after injection of cells) and the continuation of therapy during that time period, it is impossible to draw conclusions about cure rates in these studies. L2G7 efficacy was also examined in mice bearing preestablished intracranial U87 MG glioma xenografts. L2G7 (100 μg, i.p., twice weekly) given from days 5 to 52, significantly prolonged animal survival. In control mice, median survival was 39 days and all mice died from progressive tumors by day 41. In contrast, all mice treated with L2G7 survived to day 70 and 80% survived to day 90. At day 91 animals remaining alive were sacrificed and examined for tumor burden. All mice were found to have brain tumors left, which appeared to be consistent with tumor regrowth after withdrawal of L2G7 therapy.

Despite the fact that the αHGF-Nanobodies evaluated in this study did not fully inhibit c-Met–mediated phosphorylation and cell growth *in vitro*, *in vivo* these Nanobodies were found capable to give cures. These data indicate that *in vitro* functional assays are not fully predictive for assessment of the *in vivo* therapeutic potential of αHGF-targeting ligands. One aspect in favor of Nanobodies in comparison with traditional full-length mAbs is their faster and deeper tumor penetration as was previously observed for the αEGFR-Nanobody formats (18).

On the basis of the achievements described herein we think clinical evaluation of either 1E2-Alb8 or 6E10-Alb8 is justified. In such studies, the use of ^{89}Zr-immuno-PET might be of added value. Taking the complexity of signal transduction routes into account, it is uncertain whether a relationship between imaging uptake and response will be seen in patients. What might be seen, however, is a good negative predictive value of imaging, which means that there will most probably be no response when there is no Nanobody uptake in the tumor. In such way imaging might be of value to enrich the patient population that might benefit from αHGF treatment. In addition, imaging might be of value to assess the Nanobody dosage for

Published OnlineFirst February 7, 2012; DOI: 10.1158/1535-7163.MCT-11-0891

optimal tumor targeting, the optimal schedule of Nanobody administration, and cross reactivity with normal tissues to anticipate toxicity.

The potential of ^{89}Zr-immuno-PET in mAb development and applications has been shown for several mAbs directed against membrane receptors (30–33), the c-Met receptor included (34), but also for a mAb directed against a growth factor, that is, bevacizumab directed against VEGF. Like the ^{89}Zr-αHGF-Nanobodies, ^{89}Zr-bevacizumab showed selective uptake in VEGF-producing xenografts in mice (35), whereas uptake decreased when VEGF expression was inhibited by treatment with HSP90 inhibitors (36, 37), indicating a relationship between ^{89}Zr-bevacizumab tumor uptake and VEGF expression. What is more, ^{89}Zr-bevacizumab biodistribution could be imaged quantitatively and at excellent resolution, and in the mean time clinical trials have been started with ^{89}Zr-bevacizumab, as a follow-up of single-photon emission computed tomography (SPECT) studies with ^{111}In-bevacizumab in patients with melanoma (38). Although the performance of immuno-SPECT is less optimal than of immuno-PET, in these latter studies all known melanoma lesions were detected with VEGF-SPECT. In analogy, ^{89}Zr-immuno-PET might be supportive in the clinical development of the αHGF-Nanobodies.

To further improve the therapeutic potential of αHGF-Nanobodies, formatting into multitargeting Nanobodies might be an appealing option. Among others, linking αHGF-Nanobodies to our recently described αEGFR-Nanobody 7D12 might be promising (17). Like other researchers postulated; combination therapies are needed to overcome acquired resistance to inhibitors of signal transduction pathways. For instance, as recently described in lung tumors, resistance to the small-molecule epidermal growth factor receptor (EGFR) inhibitors gefitinib and erlotinib might be achieved through amplification of the *c-Met* gene (39). By combining αHGF and αEGFR units within one Nanobody construct, simultaneous blockage of both the EGFR and c-Met/HGF signal transduction pathways might result in improved therapeutic effects.

In summary, the results presented in this study showed that the Nanobodies 1E2-Alb8 and 6E10-Alb8 are capable of selectively targeting HGF-producing tumors. Furthermore, treatment of U87 MG–bearing mice with these Nanobodies resulted in inhibition of tumor growth and ultimately caused cures, indicating the therapeutic potential of αHGF-Nanobodies as cancer therapeutics in humans.

Disclosure of Potential Conflicts of Interest

J. Vercammen and H. Revets are Ablynx NV employees. J.A. Kolkman was a former employee of Ablynx NV and is presently an employee of Crucell. No potential conflicts of interest were disclosed by the other authors.

Authors' Contributions

Conception and design: M.J.W.D. Vosjan, J.A. Kolkman, G.A.M.S. van Dongen, H. Revets

Analysis and interpretation of data (e.g., statistical analysis, biostatistics, computational analysis): M.J.W.D. Vosjan, G.A.M.S. van Dongen, J. Vercammen, H. Revets

Writing, review, and/or revision of the manuscript: M.J.W.D. Vosjan, J. Vercammen, J.A. Kolkman, G.A.M.S. van Dongen, H. Revets

Administrative, technical, or material support (i.e., reporting or organizing data, constructing databases): M. Stigter-van Walsum

Grant Support

This work was in part financially supported by the Dutch Technology Foundation (M.J.W.D. Vosjan, grant 10074).

The costs of publication of this article were defrayed in part by the payment of page charges. This article must therefore be hereby marked *advertisement* in accordance with 18 U.S.C. Section 1734 solely to indicate this fact.

Received November 8, 2011; revised January 24, 2012; accepted January 25, 2012; published OnlineFirst February 7, 2012.

References

1. Cooper CS, Park M, Blair DG, Tainsky MA, Huebner K, Croce CM, et al. Molecular cloning of a new transforming gene from a chemically transformed human cell line. Nature 1984;311:29–33.
2. Bottaro DP, Rubin JS, Faletto DL, Chan AM, Kmiecik TE, Vande Woude GF, et al. Identification of the hepatocyte growth factor receptor as the c-met proto-oncogene product. Science 1991;251:802–4.
3. Birchmeier C, Birchmeier W, Gherardi E, Vande Woude GF. Met, metastasis, motility and more. Nat Rev Mol Cell Biol 2003;4:915–25.
4. Boccaccio C, Comoglio PM. Invasive growth: a MET-driven genetic programme for cancer and stem cells. Nat Rev Cancer 2006;6:637–45.
5. Hurwitz H, Fehrenbacher L, Novotny W, Cartwright T, Hainsworth J, Heim W, et al. Bevacizumab plus irinotecan, fluorouracil, and leucovorin for metastatic colorectal cancer. N Engl J Med 2004;350:2335–42.
6. Liu X, Newton RC, Scherle PA. Development of c-MET pathway inhibitors. Expert Opin Investig Drugs 2011;20:1225–41.
7. Hamers-Casterman C, Atarhouch T, Muyldermans S, Robinson G, Hamers C, Songa EB, et al. Naturally occurring antibodies devoid of light chains. Nature 1993;363:446–8.
8. Muyldermans S. Single domain camel antibodies: current status. J Biotechnol 2001;74:277–302.
9. Van Bockstaele F, Holz JB, Revets H. The development of nanobodies for therapeutic applications. Curr Opin Investig Drugs 2009;10:1212–24.
10. Conrath EK, Lauwereys M, Wyns L, Muyldermans S. Camel single-domain antibodies as modular building units in bispecific and bivalent antibody constructs. J Biol Chem 2001;276:7346–50.
11. Ulrichts H, Silence K, Schoolmeester A, de Jaegere P, Rossenu S, Roodt J, et al. Antithrombotic drug candidate ALX-0081 shows superior preclinical efficacy and safety compared with currently marketed antiplatelet drugs. Blood 2011;118:757–65.
12. Jähnichen S, Blanchetot C, Maussang D, Gonzalez-Pajuelo M, Chow KY, Bosch L, et al. CXCR4 nanobodies (VHH-based single variable domains) potently inhibit chemotaxis and HIV-1 replication and mobilize stem cells. Proc Natl Acad Sci U S A 2010;107:20565–70.
13. Roovers RC, Vosjan MJWD, Laeremans T, El Khoulati R, de Bruin RC, Ferguson KM, et al. A bi-paratopic anti-EGFR nanobody efficiently inhibits solid tumour growth. Int J Cancer 2011;129:2013–24.
14. Pant N, Marcotte H, Hermans P, Bezemer S, Frenken L, Johansen K, et al. Lactobacilli producing bispecific llama-derived anti-rotavirus proteins *in vivo* for rotavirus-induced diarrhea. Future Microbiol 2011;6:583–93.

Published OnlineFirst February 7, 2012; DOI: 10.1158/1535-7163.MCT-11-0891

15. Huang L, Gainkam LO, Caveliers V, Vanhove C, Keyaerts M, De Baetselier P, et al. SPECT imaging with ^{99m}Tc-labeled EGFR-specific nanobody for *in vivo* monitoring of EGFR expression. Mol Imaging Biol 2008;10:167–75.
16. Gainkam LO, Huang L, Caveliers V, Keyaerts M, Hernot S, Vaneycken I, et al. Comparison of the biodistribution and tumor targeting of two ^{99m}Tc-labeled anti-EGFR nanobodies in mice, using pinhole SPECT/Micro-CT. J Nucl Med 2008;49:788–95.
17. Vosjan MJWD, Perk LR, Roovers RC, Visser GWM, Stigter-van Walsum M, van Bergen en Henegouwen P, et al. Facile labelling of an anti-epidermal growth factor receptor Nanobody with ^{68}Ga via a novel bifunctional desferal chelate for immuno-PET. Eur J Nucl Med Mol Imaging 2011;38:753–63.
18. Tijink BM, Laeremans T, Budde M, Stigter-van Walsum M, Dreier T, de Haard HJ, et al. Improved tumor targeting of anti-epidermal growth factor receptor Nanobodies through albumin binding: taking advantage of modular Nanobody technology. Mol Cancer Ther 2008;7:2288–97.
19. Vosjan MJWD, Perk LR, Visser GWM, Budde M, Jurek P, Kiefer GE, et al. Conjugation and radiolabeling of monoclonal antibodies with zirconium-89 for PET imaging using the bifunctional chelate p-isothiocyanatobenzyl-desferrioxamine. Nat Protoc 2010;5:739–43.
20. Collingridge DR, Carroll VA, Glaser M, Aboagye EO, Osman S, Hutchinson OC, et al. The development of [^{124}I]iodinated-VG76e: a novel tracer for imaging vascular endothelial growth factor *in vivo* using positron emission tomography. Cancer Res 2002;60:5912–9.
21. Coppieters K, Dreier T, Silence K, de Haard H, Lauwereys M, Casteels P, et al. Formatted anti-tumor necrosis factor alpha VHH proteins derived from camelids show superior potency and targeting to inflamed joints in a murine model of collagen-induced arthritis. Arthritis Rheum 2006;54:1856–66.
22. Cao B, Su Y, Oskarsson M, Zhao P, Kort EJ, Fisher RJ, et al. Neutralizing monoclonal antibodies to hepatocyte growth factor/scatter factor (HGF/SF) display antitumor activity in animal models. Proc Natl Acad Sci U S A 2001;98:7443–8.
23. Burgess T, Coxon A, Meyer S, Sun J, Rex K, Tsuruda T, et al. Fully human monoclonal antibodies to hepatocyte growth factor with therapeutic potential against hepatocyte growth factor/c-Met-dependent human tumors. Cancer Res 2006;66:1721–9.
24. Jun HT, Sun J, Rex K, Radinsky R, Kendall R, Coxon A, et al. AMG 102, a fully human anti-hepatocyte growth factor/scatter factor neutralizing antibody, enhances the efficacy of temozolomide or docetaxel in U-87 MG cells and xenografts. Clin Cancer Res 2007;13:6735–42.
25. Gordon MS, Sweeney CS, Mendelson DS, Eckhardt SG, Anderson A, Beaupre DM, et al. Safety, pharmacokinetics, and pharmacodynamics of AMG 102, a fully human hepatocyte growth factor-neutralizing monoclonal antibody, in a first-in-human study of patients with advanced solid tumors. Clin Cancer Res 2010;16:699–710.
26. Schöffski P, Garcia JA, Stadler WM, Gil T, Jonasch E, Tagawa ST, et al. A phase II study of the efficacy and safety of AMG 102 in patients with metastatic renal cell carcinoma. BJU Int 2011;108:679–86.
27. Wen PY, Schiff D, Cloughesy TF, Raizer JJ, Laterra J, Smitt M, et al. A phase II study evaluating the efficacy and safety of AMG 102 (rilotumumab) in patients with recurrent glioblastoma. Neuro Oncol 2011;13:437–46.
28. Kim KJ, Wang L, Su YC, Gillespie GY, Salhotra A, Lal B, et al. Systemic anti-hepatocyte growth factor monoclonal antibody therapy induces the regression of intracranial glioma xenografts. Clin Cancer Res 2006;12:1292–8.
29. Lal B, Goodwin CR, Sang Y, Foss CA, Cornet K, Muzamil S, et al. EGFRvIII and c-Met pathway inhibitors synergize against PTEN-null/EGFRvIII+ glioblastoma xenografts. Mol Cancer Ther 2009;8:1751–60.
30. Perk LR, Visser OJ, Stigter-van Walsum M, Vosjan MJWD, Visser GWM, Zijlstra JM, et al. Preparation and evaluation of ^{89}Zr-Zevalin for monitoring of ^{90}Y-Zevalin biodistribution with positron emission tomography. Eur J Nucl Med Mol Imaging 2006;33:1337–45.
31. Börjesson PKE, Jauw YWS, Boellaard R, de Bree R, Comans EFI, Roos JC, et al. Performance of immuno-positron emission tomography with zirconium-89-labeled chimeric monoclonal antibody U36 in the detection of lymph node metastases in head and neck cancer patients. Clin Cancer Res 2006;12:2133–40.
32. Dijkers EC, Oude Munnink TH, Kosterink JG, Brouwers AH, Jager PL, de Jong JR, et al. Biodistribution of ^{89}Zr-trastuzumab and PET imaging of HER2-positive lesions in patients with metastatic breast cancer. Clin Pharmacol Ther 2010;87:586–92.
33. Van Dongen GAMS, Vosjan MJWD. Immuno-positron emission tomography: shedding light on clinical antibody therapy. Cancer Biother Radiopharm 2010;25:375–85.
34. Perk LR, Stigter-van Walsum M, Visser GWM, Kloet RW, Vosjan MJWD, Leemans CR, et al. Quantitative PET imaging of Met-expressing human cancer xenografts with ^{89}Zr-labelled monoclonal antibody DN30. Eur J Nucl Med Mol Imaging 2008;35:1857–67.
35. Nagengast WB, de Vries EG, Hospers GA, Mulder NH, de Jong JR, Hollema H, et al. *In vivo* VEGF imaging with radiolabeled bevacizumab in a human ovarian tumor xenograft. J Nucl Med 2007;48:1313–9.
36. Holland JP, Caldas-Lopes E, Divilov V, Longo VA, Taldone T, Zatorska D, et al. Measuring the pharmacodynamic effects of a novel Hsp90 inhibitor on HER2/neu expression in mice using Zr-DFO-trastuzumab. PLoS One 2010;5:e8859.
37. Nagengast WB, de Korte MA, Oude Munnink TH, Timmer-Bosscha H, den Dunnen WFA, Hollema H, et al. ^{89}Zr-bevacizumab PET of early antiangiogenic tumor response to treatment with HSP90 inhibitor NVP-AUY922. J Nucl Med 2010;51:761–7.
38. Nagengast WB, Hooge MNL, van Straten EME, Kruijff S, Brouwers AH, den Dunnen WFA, et al. VEGF-SPECT with ^{111}In-bevacizumab in stage III/IV melanoma patients. Eur J Cancer 2011;47:1595–602.
39. Engelman JA, Zejnullahu K, Mitsudomi T, Song Y, Hyland C, Park JO, et al. MET amplification leads to gefitinib resistance in lung cancer by activating ERBB3 signaling. Science 2007;316:1039–43.

Published OnlineFirst February 7, 2012; DOI: 10.1158/1535-7163.MCT-11-0891

Molecular Cancer Therapeutics

Nanobodies Targeting the Hepatocyte Growth Factor: Potential New Drugs for Molecular Cancer Therapy

Maria J.W.D. Vosjan, Jo Vercammen, Joost A. Kolkman, et al.

Mol Cancer Ther 2012;11:1017-1025. Published OnlineFirst February 7, 2012.